IOSR Journal of Engineering (IOSRJEN) **www.iosrjen.org**
ISSN (e): 2250-3021, ISSN (p): 2278-8719
Vol. 09, Issue 6 (June. 2019), ||S (I) || PP 69-79

TiO_2-SiO_2-C hard crystal to the Photocatalytic studies of methylene blue (MB) dye solution and IPA

K. Gayathiridevi[1] and G. Pasupathi[2*]
[1]*Department of Physics, Bharathidasan University Constituent College for Women, Orathanadu -614 625, India*
[2]*Department of Physics, A.V.V.M. Sripushpam College (Auto), Poondi -613 503, India*
Corresponding author: G. Pasupathi

Abstract: Hydrothermal synthesis of TiO_2-SiO_2-C crystals by reaction of titante-silicate-carbon layered nanocrystals and aqueous solution at 160º C from 48 h has been studied. Anisotropic growth of TiO_2-SiO_2-C crystals was observed resulting in the formation of pseudo-cubic single crystal with a dendrite shape. Growth at 160º C led to the formation of very small crystal with predominantly tetragonal structure were obtained. This study demonstrates that the anisotropic growth of these crystals can be controlled by manipulating the temperature and time of reaction and highlights the influence of growth parameters on the TiO_2-SiO_2-C crystals under hydrothermal conditions when using layered titanates with nanoparticles morphology as Ti precursor.

Keywords; Hydrothermal synthesis, Silicate, hard crystals and morphological

Date of Submission: 27-05-2019 Date of acceptance: 13-06-2019

I. INTRODUCTION

The detection and monitoring of ethanol and degradation of organic pollutants are crucial for environmental pollution control and industrial applications. Various chromatographic and spectroscopic techniques were used for the detection of hazardous solvents but the complication and sluggishness of these techniques affect their importance and vast applications [1].

Hydrothermal crystal growth corresponds to crystal growth from solution in a closed vessel, by using this, thermodynamic-stable and metastable phases can be grown. Hydrothermal method is a chemical reaction in water in a sealed pressure vessel, which is in fact a type of reaction at both high temperature and pressure. As part of catalysis—and more precisely of heterogeneous photocatalysis is an area of chemistry impacting many reactions as varied as total or mild oxidation reactions, dehydrogenation reactions, metal deposition, hydrogen transfers, etc [2].

Scrutinizing and investigation of these toxic materials in the environment is important from pollution controlling point of view. Ethanol and dyes are hazardous and toxic pollutants commonly available in the environment due to their continuous release from industries. Ethanol and dye has adverse effect on living organisms

These different reactions are mainly facing applications in the field of water and air purification treatments—targeting chemical pollutants and biological ones, self-decontaminating or self-cleaning products, organic fine chemistry as well as energy-related areas with hydrogen production from water. Activating a semiconductor leads to the promotion of an electron from the valence to the conduction band, with the simultaneous creation of a photogenerated hole within the valence band. Further, the transfer of photogenerated charge carriers to the photocatalyst surface allows redox reactions to occur with adsorbed reactants, coming from gas or liquid phase depending on the application.

The Kartheuser et al. is related to the standardization effort in the field of photocatalysis in Europe. This paper describes a proposed standardized test at the CEN level to determine the mineralization efficiency of photocatalytic media and systems (air cleaners) against a selected mixture of VOCs in a closed chamber [3].

The Simonsen et al. correlates various photoactivity tests (dye bleaching, stearic acid degradation, and gaseous acetone mineralization) of commercial TiO_2 coatings and provides promising results for future work on standardization [4].

At the catalyst surface, the redox reactions are separated into reduction and oxidative steps, involving on one hand, conduction band electrons and adsorbed electron acceptors such as, e.g., oxygen molecules $e_{CB}^{-} + A \rightarrow A^{\cdot-}$ and on the other hand, valence band holes and adsorbed electron donors such as, e.g., organic molecules or more generally the targeted pollutant hydrothermal methods were used in the synthesis of NPs and ultrafine powders and crystal growth. Reactors and autoclaves containing liquid media are subjected to 2000 psi pressure and temperature less than 200 °C and after that two routes can be followed for the formation of NPs

by hydrothermal reactions. During the hydrothermal reaction process the conditions of the reaction are very important. Solvent type, temperature, and duration affect the synthesis of the products [5].

The size of the nanoparticles increases when the reaction duration is prolonged and higher water content aids in precipitating the bigger magnetic semiconducting oxide particles. During the hydrothermal reaction, the size of the particles is controlled by nucleation and grain growth processes. Keeping the other parameters in a constant rate, their production rate is controlled by the temperature. At higher temperatures nucleation becomes faster than grain growth so that the size of the particle is decreased, but if the reaction duration is prolonged the grain growth will be advantageous in the reaction [6]

To the best of our knowledge, this reaction is the first example of crystallization of a thermodynamically stable metal oxide in an organic solvent at a temperature lower than that required by the hydrothermal reaction. In other words, this example showed that dense metal oxides can crystallize in organic solvents at temperatures lower than those required for crystallization in water [7].

The difference between these two reactions may be attributed to the activities of water present in the reaction systems, since the overall reaction is dehydration of aluminum hydroxide. However, intentional addition of a small amount of water caused the enhancement of α-alumina formation rather than the retardation expected from the equilibrium point of view. The hydrothermal deposition process is carried out at temperatures higher than 100 °C and under high atmospheric pressure conditions; an autoclave is therefore used for the process.

Actually, Yanagida et al. reported that more than 10 h are required for the complete conversion of boehmite into α-alumina, even with a reaction at 445 °C in a 0.1 N NaOH solution and in the presence of seed crystals. On the other hand, under glycothermal conditions, complete conversion of gibbsite into α-alumina is attained by the reaction at 285 °C for 4 h [8].

II. EXPERIMENTAL

Silicate (SiO_2), Titanium nitrite and potassium hydroxide are used in powder or granulated form. These materials are weighed and dissolved in pure water in advance of the preparation process. Titanium nitrite is a dense solution in its as-supplied form, and therefore the solution should be diluted before use. During the dilution of titanium nitrite with pure water, exothermic reactions take place and there is a risk that titanium nitrite will be precipitated. In order to avoid this precipitation, a slow dilution rate, with cooling, should be employed. To widen the application of this new material, TiO_2-SiO_2-C hard crystal is also tasted as a photo-catalyst for the degradation of MB dye. The newly synthesized TiO_2-SiO_2-C hard crystal exhibited high photo-catalytic activity which can open a new gateway as photo-catalyst

Crystallization of the hybrid material does not occur in most cases during the cooling phase to room temperature or upon standing for various time periods. It is also apparent that the hydrothermal parameter space is extensive, including time, temperature, fill volume, relative stoichiometries of reactants, nucleation and crystal growth rates, pH, and identity of the starting materials [9].

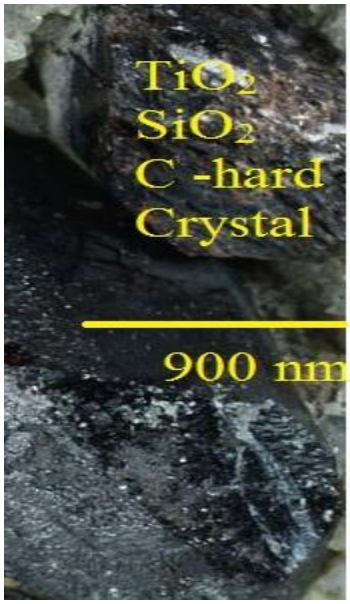

Figure 1. Grown Crystal in the length of 300 – 900 nm

Table-1 Preparation of TiO_2-SiO_2-C hard crystal

First process (nucleation)		
Ti(N Ti$(NO_3)_4$	**3.698 g**	Melted into 25 ml H_2O
SiO_2	**0.532 g**	Melted into 2 ml H_2O
Graphite	**0.250 g**	Melted into 2 ml H_2O
KOH	**1.20 g**	Melted into 7 ml H_2O
At 160 °C for 2 days		

2.1 Photocatalytic degradation

Methylene blue (MB) was employed to evaluate the photocatalytic activity of the TiO_2-SiO_2-C hard crystal. A mixture of 40 mL of 1.0×10^{-5} M dye aqueous solution and 150 mg of TiO_2-SiO_2-C hard crystal was stirred for 30 min in the dark to ensure that the adsorption/desorption of the dye on the TiO_2-SiO_2-C hard crystal surface was in equilibrium. Then the mixture was irradiated using an irradiation from a Xe lamp (CHF-XM-500W, Chang Tuo Sci-tech, Beijing). 3 mL of the dye solution was collected after irradiation times and centrifuged to separate the TiO_2-SiO_2-C hard crystal. The integrated visible-light intensity was measured to be 25 mW/cm^2 using Ultraviolet light radiometer (FZ-A). The remaining dye concentration was determined by measuring the absorption with a UV–Vis spectrophotometer (lambda 25, Perkin Elmer). The degradation or decolorization efficiency was calculated according to the equation:

$$\text{Degradation (\%)} = (C_0 - C)/C_0$$

where C_0 and C are the initial and changed concentrations of dye, respectively.

The photocatalytic activities of the prepared TiO_2-SiO_2-C hard crystal were evaluated by measuring the decomposition of gaseous iso-propanol (IPA) under Ultraviolet light irradiation. Before irradiation, the reactor was kept in the dark for 60 min to ensure an adsorption desorption equilibrium of gaseous reactants on the sample. Then the reactor was irradiated using a UV light for 2 h at room temperature. The reaction products were measured using a gas chromatograph (GC-14B, Shimadzu) equipped with a flame ionization detector [10].

III. RESULTS AND DISCUSSION

To examine the structural properties and crystal phase identifications, powder X-ray diffraction (XRD) was measured with Cu-K_α radiation in the range of 10–80º. Figure 2a shows the crystal grown of TiO_2-SiO_2-C hard crystal and Table 1 displays the list of chemical proportions it. Figure 2a displays the XRD pattern of the crystal. The observed XRD pattern exhibits well crystalline nature and mixed phases of TiO_2-SiO_2-C hard crystal for as-synthesized crystals. Several well-defined diffraction reflections are consistent with the values in the standard card (**JCPDS file no. 43-0055**) and the main diffraction peaks are indexed as (1 0 1), (6 3 3) and (8 6 0) planes of TiO_2-SiO_2-C hard crystal. Except TiO_2 crystals, no other reflections related to impurities such as TiO_2-SiO_2-C hard crystal were found in the pattern. The refinement of the TiO_2-SiO_2-C hard crystal is shown in Figure 2b, and residual plot for the refinement 2D and 3D are shown in Figure 3(a-b). Figure 4 shows the crystal structure and Unit cell parameters values of TiO_2-SiO_2-C hard crystal. The unit cell parameter of lattice planes are well agreement with the results of JCPDS (observed values) plotted in Table 2.

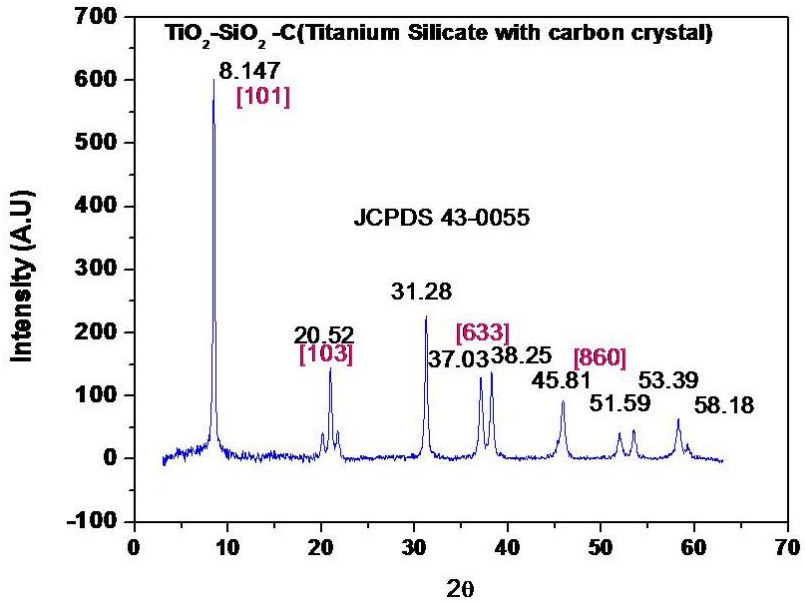

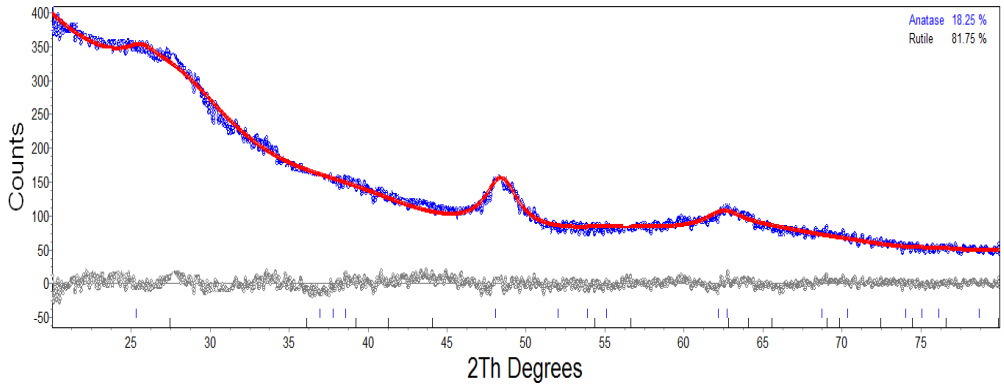

Figure. 2 (a) XRD analysis of TiO_2-SiO_2-C and (b) Refinement of TiO_2-SiO_2-C Crystal

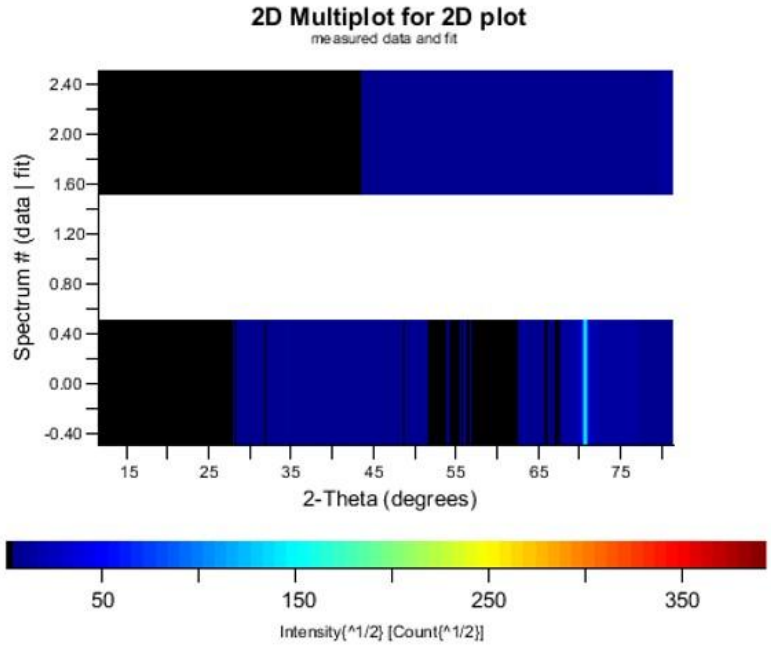

Figure 3(a) Refinement Plot of TiO_2-SiO_2-C hard crystals

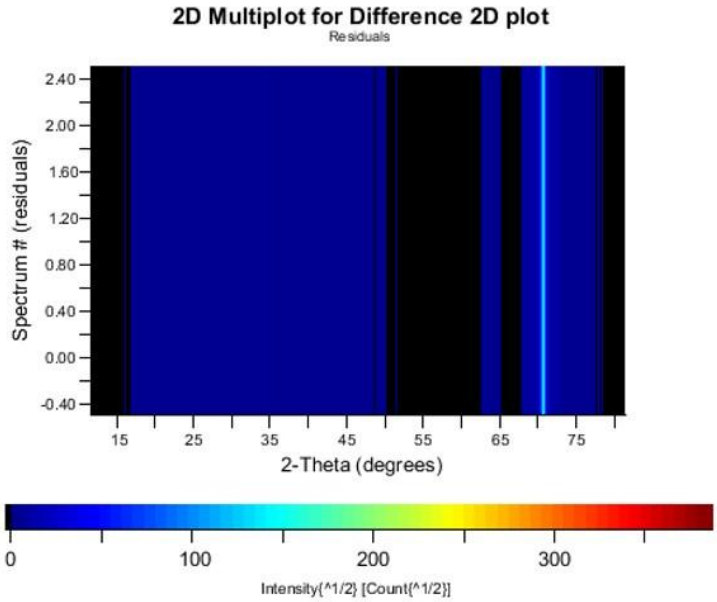

Figure 3(b) Residual Plot of TiO_2-SiO_2-C nanocrystals

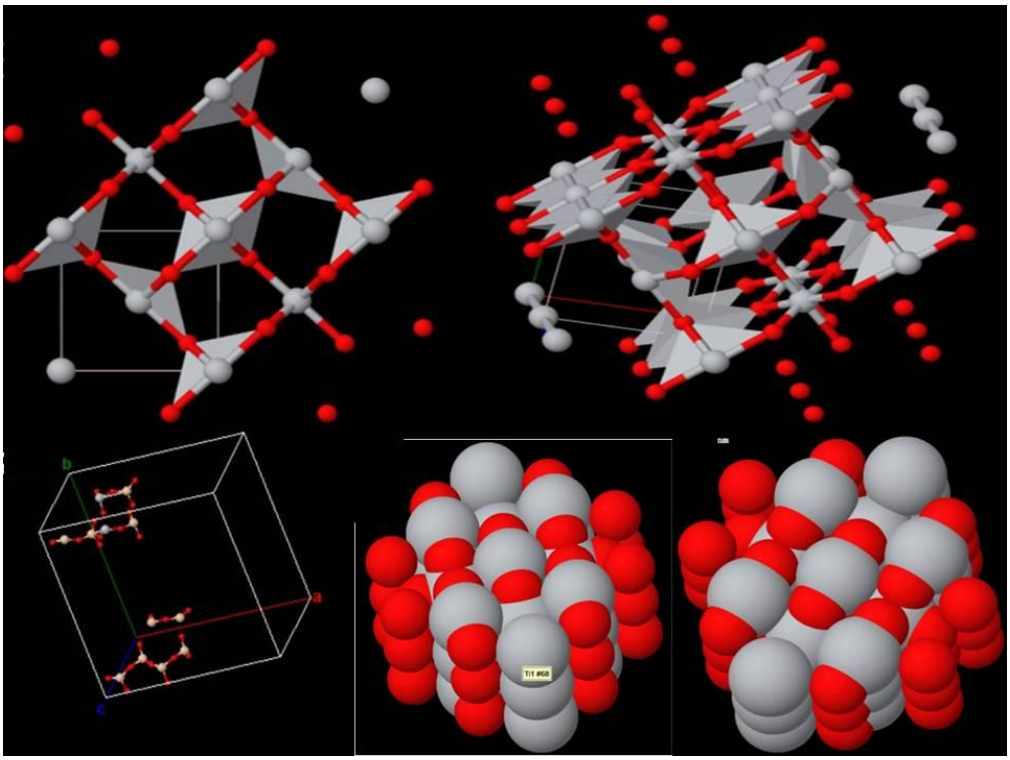

Figure 4 Crystal structures of TiO_2-SiO_2-C Crystal and its Unit cell parameters

Table -2 Structural parameters of TiO_2 – SiO_2-C Crystals (JCPDS 43-0055)

2θ		Relative Intensity	hkl	Interplaner distance (Å)		Grain size D (nm)	Lattice Parameter (Å)	
Observed	Standard JCPDS			Observed	Standard JCPDS		Calculated	JCPDS
8.147 37.03 45.81	7.926 36.10 45.067	100.00 25.23 21.82	101 633 860	11.023 2.3996 2.001	11.15 2.486 2.010	39.69 83.40 32.18	a = 20.01 c =12.99	a = 20.10 c = 13.41

The morphologies of as-synthesized TiO_2-SiO_2-C hard crystal were investigated by using FE-SEM and results are shown in Figure 5(a-b). It can be clearly seen in Figure 5(a) that the TiO_2-SiO_2-C hard crystal plates are self-assembled together to form flower like structure. The typical dimension of a single flower is about 150 nm. The SiO_2-C hard crystal was loaded in the inner-space of TiO_2 plates, indicating that TiO_2-SiO_2-C can grow directly on the surface of TiO_2 without any other process. A magnified FESEM image of TiO_2-SiO_2-C (lengths in the range of 300-900 nm and 50 nm in thickness) and TiO_2 nanoparticles (90 nm in diameter) is shown in Figure 5(b) for clarity of its morphology [11].

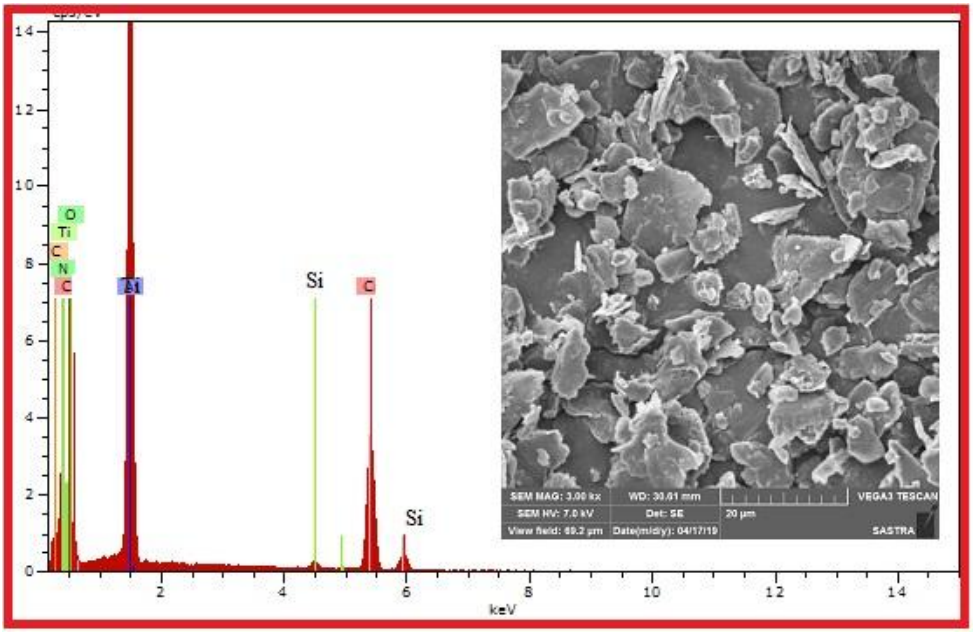

Figure 5 (a-b) SEM with EDAX analysis of TiO_2-SiO_2-C Crystals

Table 3 EDAX analysis of TiO_2-SiO_2-C nanocrystals

Element	Series	Net counts	Weight%	Atomic%
Ti	K	10090	31.43	46.62
C	K	3128	30.05	12.01
Si	K	2456	23.59	18.17
C	K	1139	10.94	18.93
O	K	1107	2.95	3.83
Si	K	107	1.04	0.44
Total			100	100

TEM images were further taken to investigate the detailed structure of the TiO_2-SiO_2-C hard crystal. Figure 6(a) shows a low-magnified TEM image of the sample. The as-synthesized composites are made up of several nanoparticles. These plates with wider bases are connected with each other in such a special fashion that they make flower-like morphologies. TiO_2 nanoparticles tightly adhere to the TiO_2-SiO_2-C hard crystal. High-magnified TEM images of an individual TiO_2 plate and TiO_2-SiO_2-C hard crystal in different areas are shown in Figures 6(b), where clear lattice fringes can be observed.

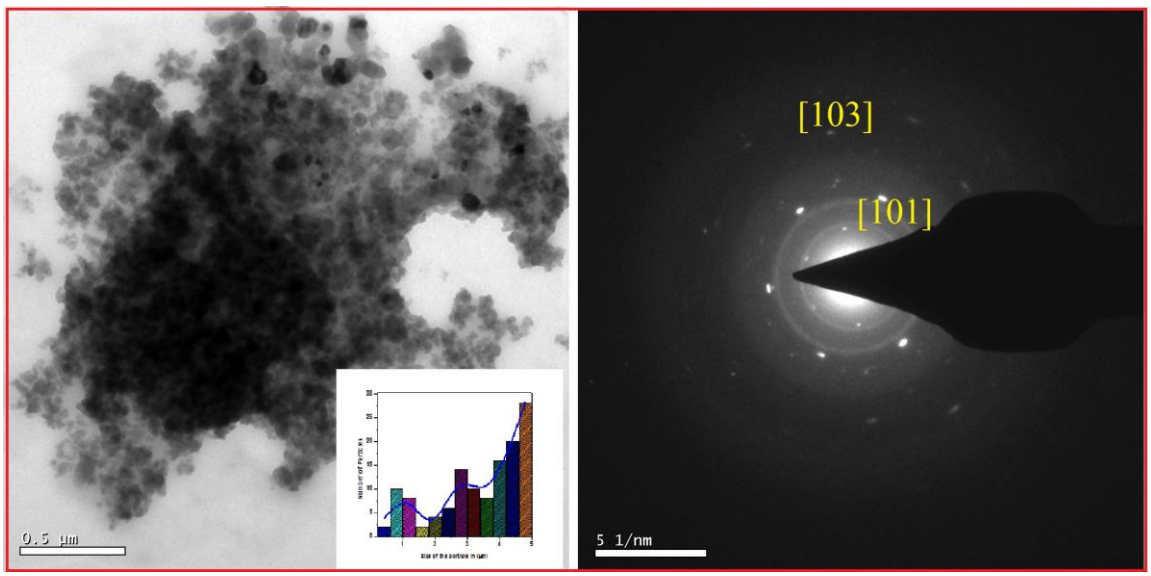

Figure 6 (a-b) TEM images of TiO_2-SiO_2-C Crystals and its SAED pattern

Figure 7(a) shows the UV-Vis absorption spectra of TiO_2-SiO_2-C hard crystal. There are two absorption bands at 365 and at 465 nm in the absorption spectra. Absorption band at 365 nm is due to transition of electrons from valance band to conduction band, which is the intrinsic absorption band of TiO_2-SiO_2-C hard crystal. This value is slightly higher than that of TiO_2-SiO_2-C hard crystal which indicates that the red shift happens in TiO_2-SiO_2-C hard crystal. This is due to a more decrease in band gap by into TiO_2-SiO_2-C hard crystal. This also implies that TiO_2-SiO_2-C hard crystal is in the regime of spatial excitonic confinement [12].

The specific surface areas of the TiO_2-SiO_2-C hard crystal have been evaluated based upon N_2 adsorption/desorption experiments. Figure 7(b) shows the N_2 dsorption/desorption isotherms for the sample. The absence of a sharp rise in nitrogen uptake near the saturation pressure (i.e., P/P_0=1) means that there are few macropores in the samples. The Brunauer-Emmett-Teller (BET) surface areas of the samples is determined to be 22.5 $m^2 g^{-1}$.

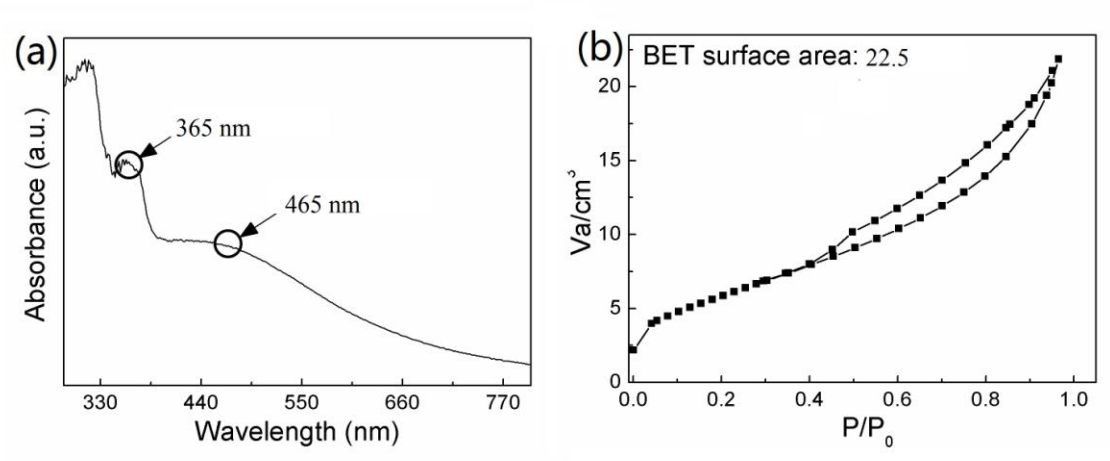

Figure 7 (a-b) UV-Vis Absorbance value with respect to wavelength (nm) and variation of Surface area P/P_0 with respect to V_a/cm^2

Photoelectrochemistry

According to the results in Figure 8(a), we choose 0.8 V bias versus SCE as applied voltages. The photocurrent responses under dark and illumination are presented in Figure 8(b). It can be clearly observed that the current abruptly increases and decreases when switch the light source on and off. The photocurrents of electrode can reach up to 0.012 mA/cm^2 under UV irradiation, which indicates that the generation, separation and transformation of photo excited electrons in TiO_2-SiO_2-C hard crystal can be obtained under the photo-irradiation.

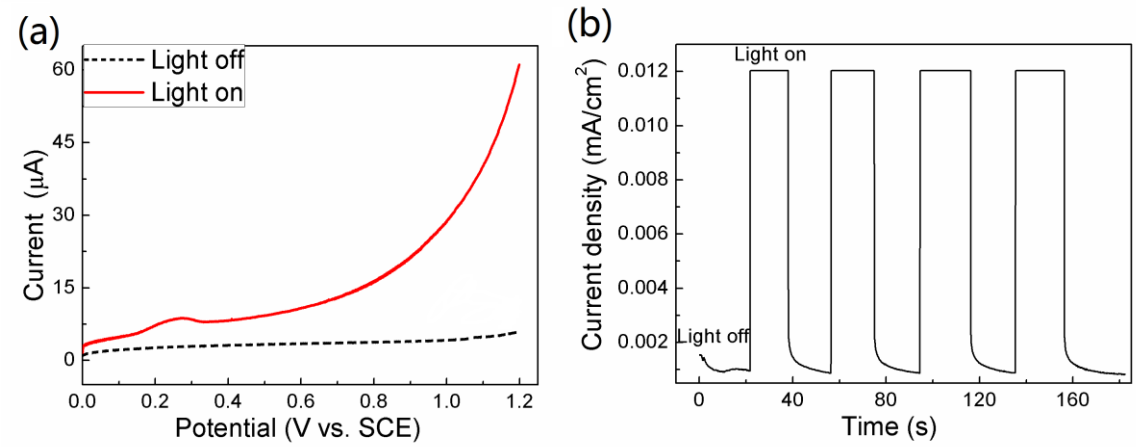

Figure 8 (a-b) Photocurrent and Time Vs Current density of TiO_2-SiO_2-C hard crystal

Photocatalytic activities

Figure 9 shows the Photo-induced formation mechanisms of electron hole pair in a semiconductor TiO_2 –SiO_2-C particle with the presence of MB dye solution and IPA. The photocurrent response experiments were

carried out under simulated solar light irradiation. Figure 10a shows a set of linear sweep voltammagrams (LSV) in dark and irradiation. It can be seen that the current keeps on a steady value (close to zero) in dark. However, with the applied potential increasing, the typical exponential increase of current can be observed under illumination. This phenomenon is attributed to photogenerated hole-electron separation resulted by the electric field [13].

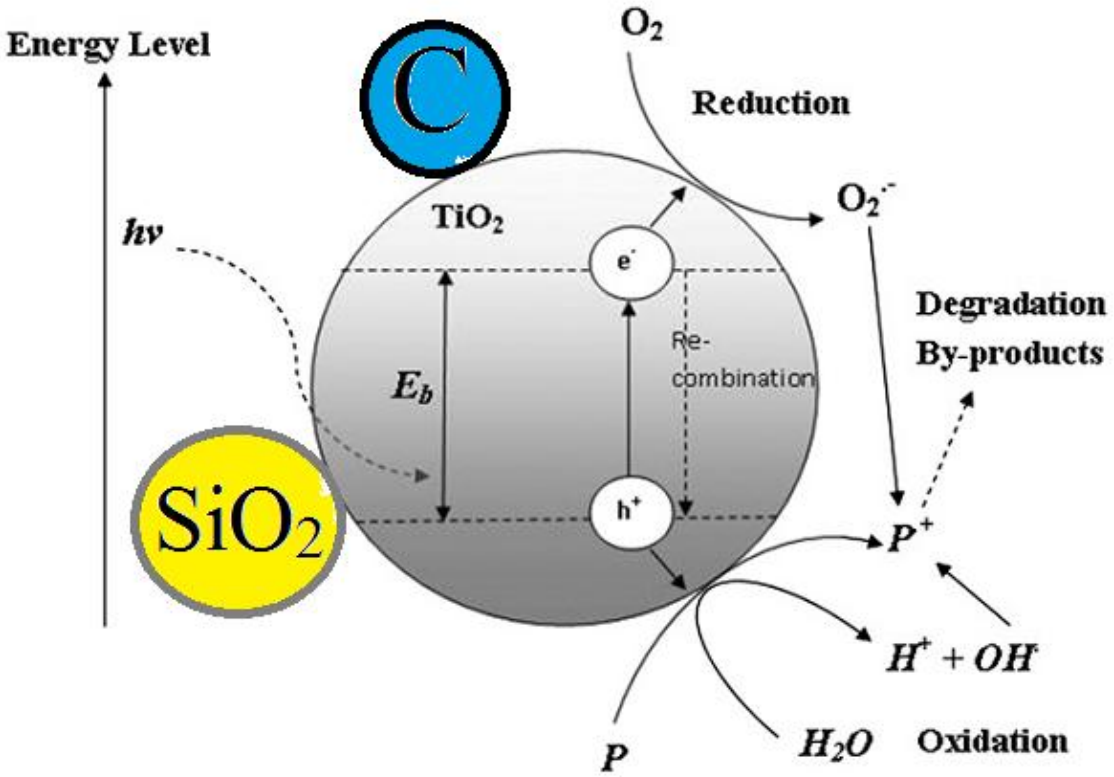

Figure 9 Photo-induced formation mechanisms of electron hole pair in a semiconductor TiO_2 –SiO_2-C particle with the presence of MB dye solution and IPA.

In order to evaluate the photocatalytic activities of the TiO_2-SiO_2-C hard crystal, methylene blue (MB) dye solution and IPA are chosen to be decomposed under irradiation. Figure 10(a) shows the photocatalytic degradation of MB as a function of irrdiation times on TiO_2-SiO_2-C hard crystal. In dark test (0-25min), a small adsorption and desorption of MB on catalyst powder can be observed. This means that the concentration of MB has attained saturation and the adsorption equilibrium was reached. When the light was turned on, the MB would be photodecomposed gradually. The degradation efficiency of 98 % with TiO_2-SiO_2-C hard crystal can be reached at 60 min of irrdiation time.

Besides the photodegradation of the MB dye solutions, gaseous organic pollution IPA was selected to evaluate the photocatalytic mineralization on the TiO_2-SiO_2-C hard crystal catalyst. Figure 10(b) shows the photocatalytic decomposition of IPA on TiO_2-SiO_2-C hard crystal under visible light ($\lambda \geq 400$ nm) irradiation. In the dark, almost no CO_2 was evolved, and the adsorption–desorption equilibrium experiments were reached in the first 40 min. This period is the adsorption process of IPA by the photocatalysts, which is similar to that of the MB dye molecules adsorption in Figure 10(a).

When the light is turned on, the acetone and CO_2 are produced gradually; the evolution yield can reached 500 and 70 *ppm* under visible light irradiation. Generally, IPA mineralization can be interpreted as follows. IPA is first photo-oxidatively dehydrogenated to acetone and eventually photo-oxidized to CO_2. Under UV irradiation, the electron and hole are generated and then transformed to the surface of TiO_2-SiO_2-C hard crystal. What the effects of TiO_2-SiO_2-C hard crystal is to collect photogenerated electrons from the conduction band of TiO_2-SiO_2-C hard crystal and improve charge separation in semiconductor-metal oxides. This can effectively inhibit the electron–hole recombination or charge recombination and therefore enhance the photocatalytic activity [14].

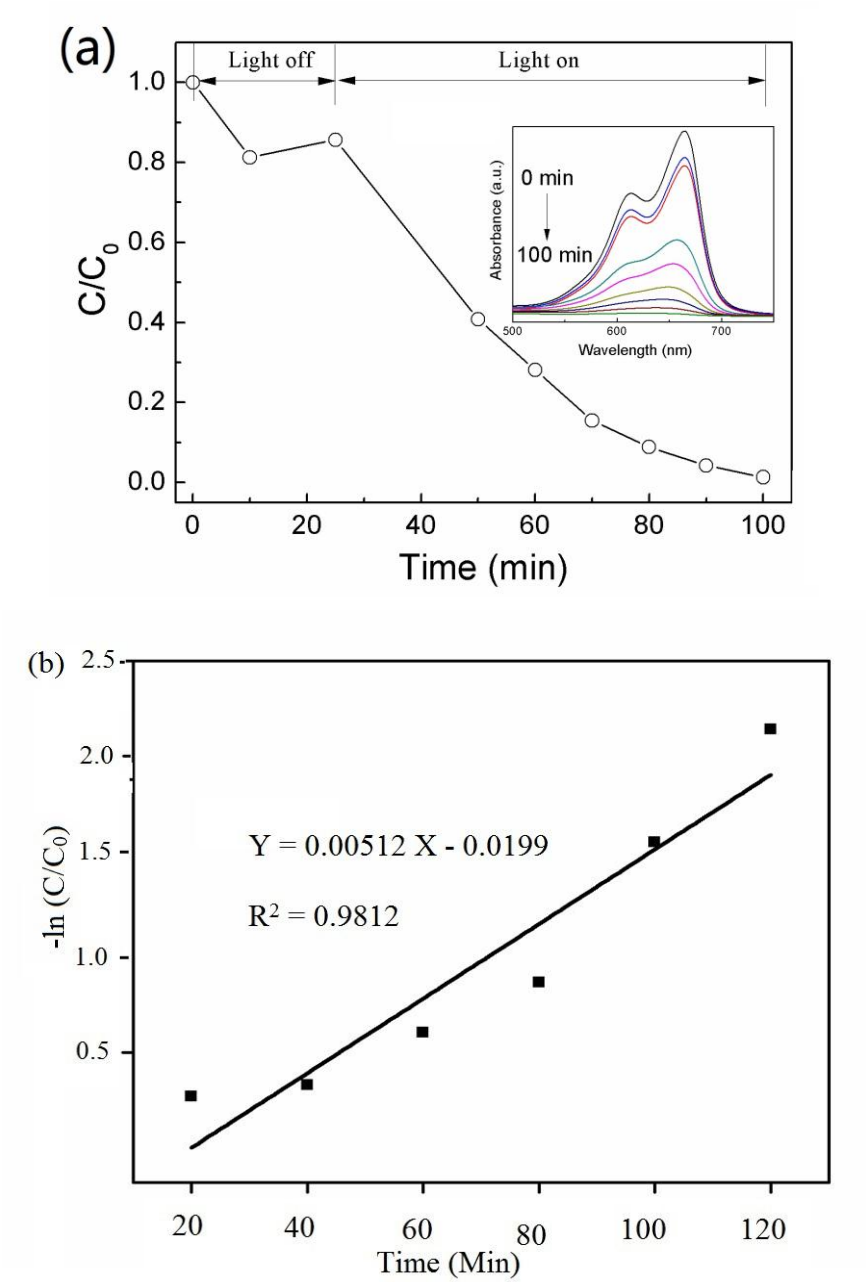

Figure 10 (a-b) Variation of Time (min) Vs C/C_0 and Variation of Time Vs –ln (C/C_0) of TiO_2-SiO_2-C hard crystal

The semiconductor TiO_2-SiO_2-C hard crystal has been widely utilized as a photocatalyst for inducing a series of reductive and oxidative reactions on its surface. This is solely contributed by the distinct lone electron characteristic in its outer orbital. When photon energy (*hv*) of greater than or equal to the bandgap energy of TiO_2-SiO_2-C hard crystal is illuminated onto its surface, usually 3.2 eV (anatase) or 3.0 eV (rutile), the lone electron will be photoexcited to the empty conduction band in femtoseconds.

Figure 10b depicts the mechanism of the electron hole pair formation when the TiO_2 particle is irradiated with adequate *hv*. The light wavelength for such photon energy usually corresponds to l < 400 nm. The photonic excitation leaves behind an empty unfilled valence band and thus creating the electron-hole pair (e^- -- h^+) [15, 16].

Kinetic Study

The Langmuir–Hinshelwood kinetic model is frequently employed to explain the kinetics of the degradation reactions of organic compounds by catalysts in aqueous solutions. The relation between the concentration of MB with IPA solution and the rate of degradation (r) is expressed by the model

$$R = -\left[\frac{dc}{dt}\right] = \frac{Kr + KadC}{1 + KadC} \text{ ------(1)}$$

where, K_{ad} is the adsorption equilibrium coefficient of MB with IPA solution onto the catalyst surface (M^{-1}), Kr is the intrinsic rate constant (M/min) and t is the irradiation time (min), while it is truly supposed that the leading mechanism of photodegradation is not adsorption, Eq.(1) can be simplified to Eq. (2) (first-order kinetics)

$$\ln(C/C_0) = -K_r K_{ad} t = -K_{app} t \text{ ----------(2)}$$

Whenever pseudo-first-order kinetics is valid, the plot of $-\ln(C/C_0)$ versus t (min) should provide a linear relationship, as stated in Eq (2). Subsequently, K_{app} can be calculated from the slope of the plot. Figure 10b depicts that the pseudo-first-order kinetic model satisfactorily fits with the obtained experimental data [17].

IV. CONCLUSION

The TiO_2-SiO_2-C hard crystal was successfully grown by 2 days from different Titania precursors via hydrothermal process. The XRD, N2 adsorption-desorption, FESEM, TEM, EDAX, and SAED pattern studies show that the addition of carbon during the synthesis does not disturb the formation of the Titanate Silicate Carbon even enhances the specific surface area, therefore confirming the effective incorporation of Carbon. The photocatalytic activity results revealed that the TiO_2-SiO_2-C hard crystal with a 1% loading of Carbon in a solution for the crystal growth under UV irradiation have higher photocatalytic degradation. Moreover, the photocatalytic degradation performance of nanocomposites is not affected by the type of titania precursor. The inclusion of the Carbon remarkably reduced the rate of electron-hole recombination, increased the surface area, and enhanced the photocatalytic activity with a longer wavelength, resulting in improved photocatalytic activities. Therefore, we conclude that the Carbon in TiO_2-SiO_2-C hard crystal is an effectual photocatalyst for degrading MB with IPA solutions under the given experimental condition

REFERENCES

[1]. Khan, Sher Bahadar, M. Faisal, Mohammed M. Rahman, and Aslam Jamal. "Exploration of CeO_2 nanoparticles as a chemi-sensor and photo-catalyst for environmental applications." Science of the total Environment, 2011; 409 (15): 2987-2992.

[2]. Ansari, S.G., Wahab, R., Ansari, Z.A., Kim, Y.S., Khang, G., Al-Hajry, A. and Shin, H.S., Effect of nanostructure on the urea sensing properties of sol–gel synthesized ZnO. Sensors and Actuators B: Chemical, 2009; 137(2): 566-573.

[3]. Kartheuser, B., Costarramone, N., Pigot, T. and Lacombe, S., NORMACAT project: normalized closed chamber tests for evaluation of photocatalytic VOC treatment in indoor air and formaldehyde determination. Environmental Science and Pollution Research, 2012; 19(9): 3763-3771.

[4]. Simonsen, M.E., Jensen, H., Li, Z. and Søgaard, E.G., Surface properties and photocatalytic activity of nanocrystalline titania films. Journal of Photochemistry and Photobiology A: Chemistry, 2008; 200(2-3): 192-200.

[5]. Mills, A., Hepburn, J., Hazafy, D., O'Rourke, C., Krysa, J., Baudys, M., Zlamal, M., Bartkova, H., Hill, C.E., Winn, K.R. and Simonsen, M.E., A simple, inexpensive method for the rapid testing of the photocatalytic activity of self-cleaning surfaces. Journal of Photochemistry and Photobiology A: Chemistry, 2013; 272: 18-20.

[6]. Huang, Q., Yu, D., Zhao, Z., Fu, S., Xiong, M., Wang, Q., Gao, Y., Luo, K., He, J. and Tian, Y., First-principles study of O-BN: A sp^3-bonding boron nitride allotrope. Journal of Applied Physics, 112(5): 053518-053527.

[7]. Nakajima, A., Koike, T., Yanagida, S., Isobe, T., Kameshima, Y. and Okada, K., Preparation and photocatalytic activity of $[PWxMo_{12-}\ xO_40]\ _3-/TiO_2$ hybrid film composites. Applied Catalysis A: General, 2010; 385(1-2): 30-135.

[8]. Yanagida, S., Nakajima, A., Sasaki, T., Isobe, T., Kameshima, Y. and Okada, K.,. Preparation and photocatalytic activity of Keggin-ion tungstate and TiO_2 hybrid layer-by-layer film composites. Applied Catalysis A: General, 2009; 366(1): 148-153.

[9]. Juan C. Rendón-Angeles, Zully Matamoros-Veloza, Adriana Matamoros Veloza, Roberto Perez-Garibay, José L. Rodriguez-Galicia, and Yanagisawa Kazumichi . Facile Synthesis of Perovskite-Structured Powders Using Barite–Celestite Ore under Hydrothermal Alkaline Conditions. Industrial & Engineering Chemistry Research **2017;** 56 (36): 9942-9952.

[10]. Liao, Y.H.B., Wang, J.X., Lin, J.S., Chung, W.H., Lin, W.Y. and Chen, C.C., 2011. Synthesis, photocatalytic activities and degradation mechanism of Bi_2WO_6 toward crystal violet dye. Catalysis today, 2011; 174(1):148-159.

[11]. Yanagida, T., Horizontal symmetry and masses of neutrinos. Progress of Theoretical Physics, 1980; 64(3): 1103-1105.
[12]. Liu, B.J., Torimoto, T. and Yoneyama, H., Photocatalytic reduction of carbon dioxide in the presence of nitrate using TiO_2 nanocrystal photocatalyst embedded in SiO_2 matrices. Journal of Photochemistry and Photobiology A: Chemistry, 1998; 115(3): 227-230.
[13]. An, T., Chen, J., Nie, X., Li, G., Zhang, H., Liu, X. and Zhao, H., Synthesis of carbon nanotube–anatase TiO_2 sub-micrometer-sized sphere composite photocatalyst for synergistic degradation of gaseous styrene. ACS applied materials & interfaces, 2012; 4(11): 5988-5996.
[14]. Panayotov, D.A., Paul, D.K. and Yates, J.T., Photocatalytic Oxidation of 2-Chloroethyl Ethyl Sulfide on TiO_2− SiO_2 Powders. The Journal of Physical Chemistry B, 2003; 107(38): 10571-10575.
[15]. Nakano, K., Obuchi, E., Takagi, S., Yamamoto, R., Tanizaki, T., Taketomi, M., Eguchi, M., Ichida, K., Suzuki, M. and Hashimoto, A., Photocatalytic treatment of water containing dinitrophenol and city water over TiO_2/SiO_2. Separation and purification technology, 2004; 34(1-3): 67-72.
[16]. Kaviyarasu, K., N. Geetha, K. Kanimozhi, C. Maria Magdalane, S. Sivaranjani, A. Ayeshamariam, J. Kennedy, and M. Maaza. "In vitro cytotoxicity effect and antibacterial performance of human lung epithelial cells A549 activity of zinc oxide doped TiO_2 nanocrystals: investigation of bio-medical application by chemical method." Materials Science and Engineering: C, 2017; 74: 325-333.
[17]. Hosseini-Zori, Maryam. "Co-doped TiO_2 nanostructures as a strong antibacterial agent and self-cleaning cover: Synthesis, characterization and investigation of photocatalytic activity under UV irradiation." Journal of Photochemistry and Photobiology B: Biology, 2018; 178: 512-520.

G. Pasupathi. "TiO2-SiO2-C hard crystal to the Photocatalytic studies of methylene blue (MB) dye solution and IPA." IOSR Journal of Engineering (IOSRJEN), vol. 09, no. 06, 2019, pp. 69-79.